# Fermi Surface Nesting with Heavy Quasiparticles in the Locally Noncentrosymmetric Superconductor $CeRh_2As_2$

Yi Wu[1†], Yongjun Zhang[2†], Sailong Ju[3], Yong Hu[3], Yanen Huang[1], Yanan Zhang[1], Huali Zhang[1], Hao Zheng[1], Guowei Yang[1], Evrard-Ouicem Eljaouhari[4], Baopeng Song[2], Nicholas C. Plumb[3], Frank Steglich[1,5], Ming Shi[1,3], Gertrud Zwicknagl[4,5], Chao Cao[1*], Huiqiu Yuan[1,6,7*], and Yang Liu[1,6*]

[1]*Center for Correlated Matter and School of Physics, Zhejiang University, Hangzhou 310058, China*
[2]*Institute for Advanced Materials, Hubei Normal University, Huangshi 435002, China*
[3]*Swiss Light Source, Paul Scherrer Institut, CH-5232 Villigen PSI, Switzerland*
[4]*Institut for Mathematische Physik, 38106 Braunschweig, Germany*
[5]*Max Planck Institute for Chemical Physics of Solids, 01187 Dresden, Germany*
[6]*Collaborative Innovation Center of Advanced Microstructures, Nanjing University, Nanjing 210093, China*
[7]*State Key Laboratory of Silicon Materials, Zhejiang University, Hangzhou 310058, China*

(Received 14 August 2024; accepted manuscript online 4 September 2024)

The locally noncentrosymmetric heavy fermion superconductor $CeRh_2As_2$ has attracted considerable interests due to its rich superconducting phases, accompanied by possible quadrupole density wave and pronounced antiferromagnetic excitations. To understand the underlying physics, here we report measurements from high-resolution angle-resolved photoemission. Our results reveal fine splittings of the conduction bands related to the locally noncentrosymmetric structure, as well as a quasi-two-dimensional Fermi surface (FS) with strong $4f$ contributions. The FS shows signs of nesting with an in-plane vector $\boldsymbol{q}_1 = (\pi/a, \pi/a)$, which is facilitated by the heavy bands near $\bar{X}$ arising from the characteristic conduction-$f$ hybridization. The FS nesting provides a natural explanation for the observed antiferromagnetic spin fluctuations at $(\pi/a, \pi/a)$, which might be the driving force for its unconventional superconductivity. Our experimental results can be reasonably explained by density functional theory plus dynamical mean field theory calculations, which can capture the strong correlation effects. Our study not only provides spectroscopic signature of the key factors underlying the field-induced superconducting transition, but also uncovers the critical role of FS nesting and lattice Kondo effect in the underlying magnetic fluctuations.

DOI: 10.1088/0256-307X/41/9/097403

The recent discovery of heavy fermion (HF) superconductivity ($T_c \sim 0.26\,K$) in $CeRh_2As_2$ has attracted broad interests.[1] The large specific jump at $T_c$ indicates that the Cooper pairs are formed out of the heavy quasiparticles as a result of the Kondo effect.[1] A remarkable field-induced first-order transition within the superconducting phase can be observed for a magnetic field applied along the $c$ axis,[1] which was attributed to an even-odd parity transition as a result of the local noncentrosymmetricity at the Ce sites.[1–10] Such a parity transition is extremely rare for superconductors. A small interlayer hopping and larger Rashba-like spin-orbit coupling (SOC, due to the local noncentrosymmetricity) are thought to be essential for the parity transition of superconductivity.[1,3–7,11] It is therefore imperative to unravel the electronic structure underlying the peculiar superconductivity, particularly the influences of the interlayer coupling and the locally noncentrosymmetric structure.

Another key problem in $CeRh_2As_2$ is the origin of the observed antiferromagnetic (AFM) fluctuations[12] or order,[13,14] as well as the nature of the transition at $T_0 \sim 0.4\,K$.[1,14,15] Pronounced AFM excitations observed from inelastic neutron scattering (INS)[12] and possible AFM order below $T_c$ inferred from nuclear quadrupole resonance[13] point towards a magnetically driven superconductivity in $CeRh_2As_2$, similar to other prototypical HF superconductors, such as $CeCu_2Si_2$[16,17] and $CeCoIn_5$.[18] A very recent study from muon spin relaxation ($\mu$SR) further revealed the microscopic coexistence of magnetism and superconductivity.[14] Interestingly, quasi-two-dimensional (2D) magnetic excitations were observed at $\boldsymbol{q}_0 = (\pi/a, \pi/a)$ in INS,[12] which is often related to the nesting of Fermi surface (FS).[19] Alternatively, the transition at $T_0$ was proposed to be into an unconventional quadrupole density wave (QDW) based on renormalized band calculations,[15,20] where the nesting of the FS (involving itinerant $4f$ bands) can also be important. Nevertheless, how the itinerant heavy quasiparticles develop and can account for the spin/charge order in $CeRh_2As_2$ remains an open problem.[21–23]

†These authors contributed equally to this work.
*Corresponding authors. Email: ccao@zju.edu.cn; hqyuan@zju.edu.cn; yangliuphys@zju.edu.cn
© 2024 Chinese Physical Society and IOP Publishing Ltd

In this Letter, we report measurements of the quasiparticle dispersion and FS in $CeRh_2As_2$, from angle-resolved photoemission spectroscopy (ARPES). Although there have been a few theoretical studies on the electronic structure,[4,7,15,24,25] high-resolution ARPES measurement is still needed. Our experimental results are also supported by state-of-art calculations from density functional theory (DFT) plus dynamical mean-field theory (DMFT), and such a combination allows us to develop a thorough understanding of the correlation effects. Details of crystal growth, characterizations, ARPES measurements and calculations can be found in the Supplementary Material[26] (also see Refs. [27–38] and references therein).

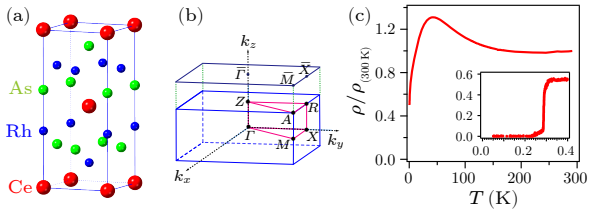


**Fig. 1.** (a) Crystal structure of $CeRh_2As_2$. (b) The bulk (bottom) and projected surface (top) BZ's. (c) Resistivity vs temperature. Inset is a zoomed-in view near $T_c$.

$CeRh_2As_2$ crystallizes in a $CaBe_2Ge_2$-type tetragonal structure [see Fig. 1(a) and the Brillouin zone (BZ) in Fig. 1(b)]: each Ce layer is sandwiched by alternating Rh–As–Rh and As–Rh–As trilayers, which break the local inversion symmetry at the Ce sites, although the global inversion center still exists. The sample quality is confirmed by the temperature-dependent resistivity [Fig. 1(c)], which exhibits a broad maximum at $T^* \sim 40$ K and a superconducting transition at $T_c \sim 0.24$ K (zero resistivity). Note that the cleaved surfaces for ARPES measurements probably consist of small domains with different surface terminations, whose sizes are smaller than the beam spot (see Fig. S2 in the Supplementary Material[26]). While the mixed surface terminations lead to considerable spectral broadening, they also indicate that the strong features observed experimentally should be bulk states, as verified by comparison with the following calculations.

Figures 2(a) and 2(b) show the dispersion of conduction bands along $\bar{\Gamma}$–$\bar{M}$ taken with two representative photon energies (additional data and calculations in Figs. S3 and S4 of the Supplementary Material[26]). Except from the flat $4f$ bands at the Fermi level ($E_F$) and $-0.27$ eV, which will be discussed later, the dispersive conduction (non-$4f$) bands well below $E_F$ consist of large electron pockets centered at $\bar{M}$ (denoted as $\alpha$), as well as both hole ($\beta$) and shallow electron ($\gamma$) pockets centered at $\bar{\Gamma}$ [blue arrows in Fig. 2(a)]. The observed conduction bands away from $E_F$ can be compared reasonably well with the DFT calculations [Figs. 2(c) and 2(d)], which treat Ce $4f$ electrons as core electrons (core-$4f$ calculation). For example, the $\alpha$ and $\beta$ bands show small differences for $k_z = 0$ and $k_z = \pi/c$ [compare Figs. 2(a) and 2(c) with Figs. 2(b) and 2(d)], and there is an M-shape band near $-1$ eV at $k_z = 0$ [green dashed circles in Figs. 2(a) and 2(c)]. The $k_z$ dispersion can be further verified by the photon-energy dependent scan in Fig. 2(e), where the band positions at $E_F$ exhibit weak periodic modulation with $k_z$, allowing for an estimation of the inner potential $V_0 \approx 15$ eV. Despite some $k_z$-dependent intensities caused by weak $k_z$ dispersion, the dominant spectral features are nearly vertical and extend along the $k_z$ direction, indicating its quasi-2D nature. The quasi-2D FS implies dominant intralayer hopping compared to the weak interlayer hopping, which is thought to be crucial for the high-field odd-parity superconducting phase in $CeRh_2As_2$.[3–7]

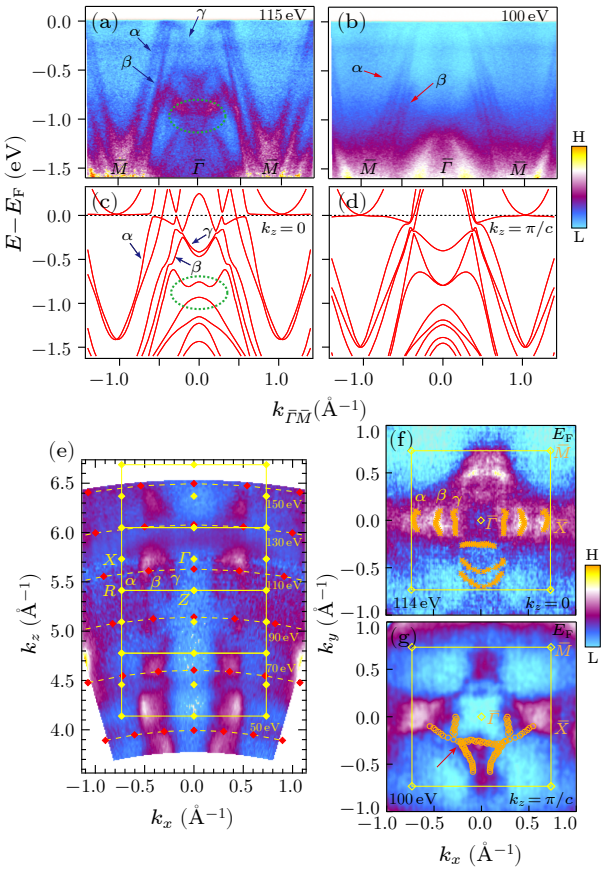


**Fig. 2.** (a)–(d) ARPES spectra taken with 115 eV (a) and 100 eV (b) photons along the $\bar{\Gamma}$–$\bar{M}$ direction, in comparison with DFT calculations at $k_z = 0$ (c) and $\pi/c$ (d). (e) The $k_x$–$k_z$ map at $E_F$ along the in-plane $\bar{\Gamma}$–$\bar{X}$ direction ($k_x$) using vertically polarized photons. The yellow rectangles (with points) mark the BZ boundaries. Red dashed curves represent various $k_z$ cuts corresponding to different photon energies. [(f), (g)] In-plane FS maps from 114 eV (f) and 100 eV (g) photons. The orange crosses and circles in the lower halves of the FS maps indicate experimentally extracted Fermi contours. The color bars for the image plots are indicated on the right (L: low intensity, H: high intensity).

From the DFT calculations, both $\alpha$ and $\beta$ bands actually consist of two closely spaced (or split) bands, which can be clearly identified in the ARPES data [red arrows in Fig. 2(b)]. Direct observation of these fine features demonstrates the high spectral quality. These splittings are closely related to the $CaBe_2Ge_2$-type crystal struc-

ture, which hosts alternating Rh–As–Rh and As–Rh–As trilayers that break the local inversion symmetry of the Ce layers. Indeed, calculations assuming the $ThCr_2Si_2$-type structure with identical As–Rh–As trilayers, where the centrosymmetricity of the Ce layers is restored, does not exhibit such band splitting (see Fig. S5 in the Supplementary Material [26]). Therefore, these fine splittings are direct manifestations of the local noncentrosymmetricity of the Ce layers, which is intimately connected to the multiple superconducting phases in $CeRh_2As_2$. [1–10] We note that for the HF compounds with the $ThCr_2Si_2$-type centrosymmetric structure, e.g., $CeRu_2Si_2$ [39] and $CeCu_2Si_2$, [40] no similar band splittings have been reported.

The in-plane FS maps at $k_z = 0$ and $\pi/c$ are shown in Figs. 2(f) and 2(g), where the Fermi contours extracted experimentally (yellow crosses/circles) are overlaid in the lower halves of the experimental data. For $k_z = 0$ [Fig. 2(f)], the $\alpha$ and $\beta$ pockets exhibit diamond shape (more discussions in the following), while the inner $\gamma$ pocket appears to be square-like. By contrast, at $k_z = \pi/c$ [Fig. 2(g)], the $\alpha$ and $\beta$ pockets become very close and lead to one large diamond-shaped pocket (highlighted by a red arrow), joined by strong spectral features near $\bar{X}$.

Now we discuss the $4f$ states near $E_F$. We employed resonant ARPES measurement at 120 eV (the Ce $N$ edge), where the photoemission cross section for the $4f$ states near $E_F$ is largely enhanced. [41] The results [Fig. 3(a)] show that the $4f$ states near $E_F$ actually consist of the $4f^1_{5/2}$ peak near $E_F$ ($J = 5/2$) and the spin-orbit split $4f^1_{7/2}$ peak at $\sim -0.27$ eV ($J = 7/2$), which can be clearly seen in the energy distribution curves (EDCs). These Kondo peaks arise from the many-body Kondo process and develop into propagating heavy bands in a periodic lattice. [39,42,43] A zoomed-in view of the quasiparticle dispersion near $E_F$, shown in Fig. 3(b) reveals a nearly flat $4f^1_{5/2}$ band and a clear bending of the conduction bands (black arrow), due to hybridization between conduction and $4f$ electrons ($c$–$f$ hybridization). [44–49] To compare with experiments, we perform both DFT and DFT + DMFT calculations [see Figs. 3(c)–3(e)]. Although the core-$4f$ DFT calculation [Fig. 3(c)] can capture the conduction bands away from $E_F$, it cannot account for the correlated $4f$ bands near $E_F$. By contrast, the valence-$4f$ calculation [Fig. 3(d)], which treats $4f$ electrons as valence electrons with Hubbard $U$, can generate $4f$ bands near $E_F$, but their position and dispersion are very different from experiments, such deviation for the $4f$ bands is unsurprising in strongly correlated HF systems. Figure 3(e) shows the calculated $k$-resolved spectral function from DFT + DMFT, which reveals good agreement with experiments: the weakly dispersive $4f$ band and the bending of conduction bands near $E_F$ can be reproduced well. The bending of conduction bands [black arrows in Figs. 3(b) and 3(e)], caused by the $c$–$f$ hybridization, is also accompanied by an increase of $4f$ weight, leading to characteristic "hot" spots near $E_F$ [Fig. 3(b)]. Figures 3(f) and 3(g) demonstrate the comparison between ARPES and DFT + DMFT along $\bar{\Gamma}$–$\bar{X}$ at $k_z = \pi/c$, where good agreement can be found. In particular, the heavy hole band near $\bar{X}$ [red arrows in Figs. 3(f) and 3(g)] gives rise to large density of states (DOS) at $E_F$. This DOS peak, akin to a 2D van Hove singularity (VHS), is driven by $c$–$f$ hybridization characteristic of HF systems and is different from the conduction-band VHS at $k_z = 0$ discussed in an independent ARPES paper. [50]

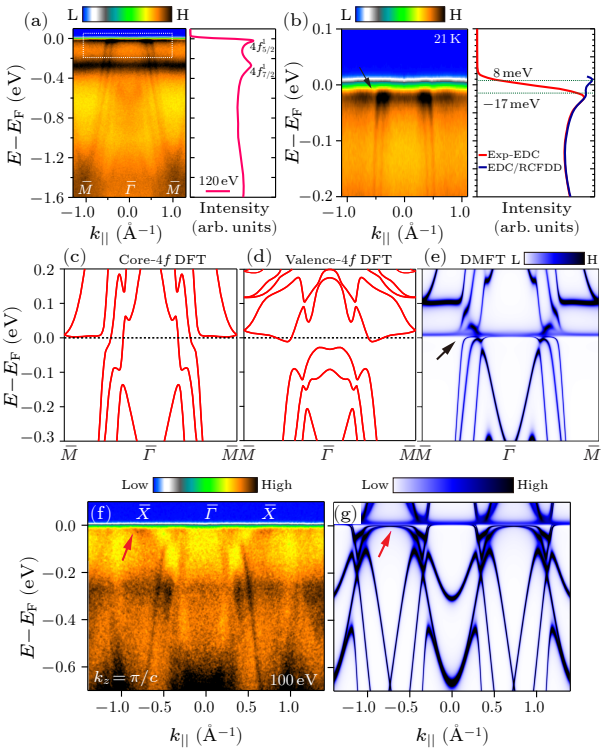


**Fig. 3.** (a) Resonant ARPES spectra (left) along $\bar{\Gamma}$–$\bar{M}$ and its corresponding momentum-integrated EDC (right). (b) Zoom-in view of (a) near $E_F$. Right: the EDC (red) and its division by RC-FDD (blue). The EDCs in [(a), (b)] are integrated from −1.2 to 1.2 Å$^{-1}$. (c)–(e) Band dispersion from core-$4f$ (c), valence-$4f$ (d) DFT calculations and $k$-resolved spectral function from DFT + DMFT calculations (e), for comparison with (b). The electron-like $\gamma$ bands at $\bar{\Gamma}$ are not obvious in the experimental data likely due to small photoemission matrix elements. [(f), (g)] ARPES spectrum along $\bar{\Gamma}$–$\bar{X}$ at $k_z = \pi/c$ (f), in comparison with DFT + DMFT calculation (g).

The proposed QDW at $T_0$ in $CeRh_2As_2$ was attributed to mixing of the ground-state and first excited $4f$ doublets due to strong Kondo effect, [15] which effectively leads to a quartet ground state for $4f$ electrons, similar to cubic systems with quadrupole order, e.g., $CeB_6$. [51–53] Since the crystal electric field (CEF) states of $4f$ electrons are manifest through the fine satellite structures in the Kondo peaks, [45,54–56] we divided the ARPES spectra by the resolution-convoluted Fermi–Dirac distribution (RC-FDD) [see Fig. S6 in the Supplementary Material [26]], which recovers the full spectral function near $E_F$. The result [right panel in Fig. 3(b)] reveals two $4f$ peaks at $\sim 8$ meV and $\sim -17$ meV, respectively. Previous studies suggest that the energy separation between the ground state $\Gamma^1_7$ and first excited doublet $\Gamma_6$ (second excited doublet $\Gamma^2_7$) is

$\Delta_1 \sim 2.6\,\text{meV}$ ($\Delta_2 \sim 15.5\,\text{meV}$).[1,15,57] Therefore, the satellite peak at $-17\,\text{meV}$ could correspond to CEF excitations related to $\Gamma_7^2$, while the peak at $\sim 8\,\text{meV}$ might contain broadened contributions from both $\Gamma_7^1$ and $\Gamma_6$, due to limited energy resolution. The observed fine structures of the $4f_{5/2}^1$ Kondo peak, as well as their temperature evolution (see Fig. S7 in the Supplementary Material[26]), are overall consistent with the proposed CEF scheme.[1,15,57]

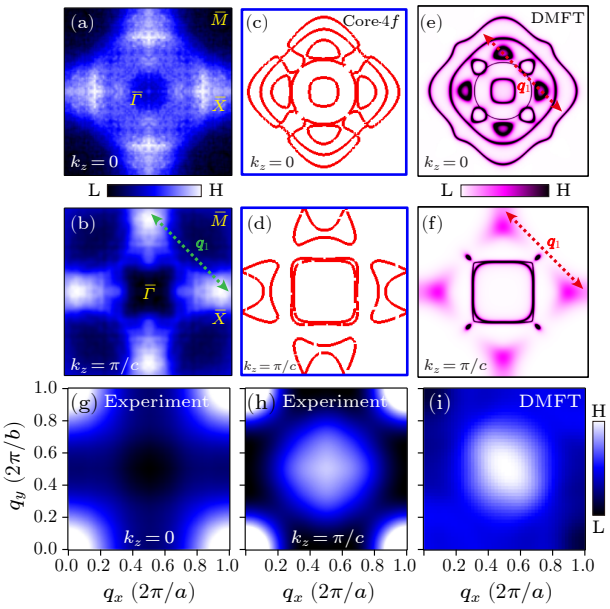


**Fig. 4.** [(a), (b)] In-plane experimental FS maps within first BZ at $k_z = 0$ (a) and $\pi/c$ (b). Here the maps are symmetrized according to the bulk $C_4$ rotation. (c)–(f) The calculated in-plane FS's from the core-4$f$ DFT [(c), (d)] and DFT + DMFT [(e), (f)] calculations. The dashed arrows in [(b), (e), (f)] indicate the nesting vector $\boldsymbol{q}_1$. [(g), (h)] Autocorrelation $C(\boldsymbol{q}, 0)$ of the ARPES FS maps for $k_z = 0$ (g) and $\pi/c$ (h). (i) The quadrupolar susceptibility $\chi^{qd}(\boldsymbol{q})$ calculated from DFT + DMFT.

Figures 4(a)–4(f) show the detailed comparison between the experimental and theoretical FS's. While the core-4$f$ DFT calculation appears to explain the shape of the experimental FS at $k_z = 0$ [compare Figs. 4(a) and 4(c)], it fails to account for the FS at $k_z = \pi/c$ [compare Figs. 4(b) and 4(d)]. By contrast, the DFT + DMFT calculations in Figs. 4(e) and 4(f) show better agreement with experiments at both $k_z$ cuts, particularly the large diamond-shaped pocket and the strong spectral feature near $\bar{X}$ at $k_z = \pi/c$ [compare Figs. 4(b) and 4(f)]. Note that the DFT + DMFT FS at $k_z = 0$ has the shape similar to the core-4$f$ FS [compare Figs. 3(c) and 3(e)], although the pocket sizes are slightly smaller due to band bending from $c$–$f$ hybridization [see Figs. 3(b) and 3(e)]. Therefore, the experimental FS and its anisotropic 4$f$ weight is a direct consequence of the band-dependent $c$–$f$ hybridization,[58] which is well captured by DFT + DMFT calculations.

Both the experimental and theoretical FS maps exhibit signatures of nesting. A nesting vector $\boldsymbol{q}_1 \approx (\pi/a, \pi/a)$, marked by dashed arrows in Figs. 4(b) and 4(f), can connect the heavy quasiparticles with high DOS near $\bar{X}$ at $k_z = \pi/c$. This vector can also link the parallel portions of the outer $\alpha$ pocket at $k_z = 0$, as indicated by a red dashed arrow in Fig. 4(e). For quantitative analysis of FS nesting, we calculate the autocorrelation $C(\boldsymbol{q}, \omega)$ of the ARPES spectral function $A(\boldsymbol{k}, \omega)$ via[59–61]

$$C(\boldsymbol{q}, \omega) = \sum_{\boldsymbol{k}} A(\boldsymbol{k}, \omega) A(\boldsymbol{k} + \boldsymbol{q}, \omega),$$

where the summation is over the first BZ. The 2D results for the $k_z = 0$ and $k_z = \pi/c$ FS maps are shown in Figs. 4(g) and 4(h), respectively. A pronounced peak at $\boldsymbol{q} = (\pi/a, \pi/a)$ in Fig. 4(h) indicates FS nesting at this wave vector. Note that the expected peak at $(\pi/a, \pi/a)$ is not obvious in the $k_z = 0$ map in Fig. 4(g). This is due to the weak photoemission intensity of the outer $\alpha$ pocket along the diagonal $\bar{\Gamma}$–$\bar{M}$ direction [see Fig. 4(a)], where large contributions to the FS nesting are expected [red dashed arrow in Fig. 4(e)]. The FS nesting can be further verified by the DFT + DMFT calculation in Fig. 4(i), where the quadrupolar susceptibility $\chi^{qd}(\boldsymbol{q})$ using the three-dimensional electronic structure obtained from the DFT + DMFT calculation is plotted.[26] The result shows a strong peak at $\boldsymbol{q}_1 = (\pi/a, \pi/a)$, implying FS instability or strong fluctuation associated with $\boldsymbol{q}_1$.

In HF systems, the nesting of FS with heavy quasiparticles is often necessary for the strong magnetic excitations and spin fluctuations,[17,62,63] which could eventually lead to HF superconductivity. At the nesting vector (usually the same as the AFM ordering vector in parent compound), spin resonances have been detected,[63–65] which are closely connected to the superconducting order parameter. Interestingly, the observed FS nesting at $\boldsymbol{q}_1 = (\pi/a, \pi/a)$ in $CeRh_2As_2$ matches well with the quasi-2D AFM excitations at $(\pi/a, \pi/a)$ from INS measurements.[12] It is therefore desirable to check if spin resonances can be observed in such experiments at this vector upon entering the superconducting state.

In principle, the proposed QDW at $T_0$ also requires nesting of the FS.[15] The coexistence of strong magnetic excitations and possible quadrupole order in $CeRh_2As_2$ is reminiscent of the famous compound $URu_2Si_2$,[66] where a "hidden-order" transition at $\sim 17.5\,\text{K}$ could be attributed to certain type of multipole order,[67,68] accompanied by strong magnetic excitations observed by INS.[69–71] In addition, extensive ARPES studies of $URu_2Si_2$ revealed partial gapping of the nested FS across the hidden-order transition,[72–78] although the underlying mechanism remains unsettled. Therefore, $CeRh_2As_2$ could provide another interesting platform to study the delicate interplay between orbital and magnetic degrees of freedom in correlated $f$-electron systems,[14] as well as their connection with the unconventional superconductivity.[19,79]

According to theory, a large Rashba-type SOC due to local noncentrosymmmetricity and a small interlayer hopping are both crucial for realizing the field-induced parity transition in $CeRh_2As_2$.[3–7] Our observation of band splittings caused by the locally noncentrosymmetric struc-

ture [Fig. 2(a) and 2(b)] and a quasi-2D FS with strong $4f$ contributions [see Fig. 2(e) and Fig. S8 in the Supplementary Material[26]] provides spectroscopic evidence of these electronic properties, although our ARPES measurements were performed above $T_c$. The quantitative information obtained herein lays the basis for more in-depth investigations in the future.

In summary, our high-resolution ARPES measurements on $CeRh_2As_2$, in combination with DFT + DMFT calculations, demonstrate that the Ce $4f$ electrons play a significant role in the FS due to band-dependent $c$–$f$ hybridization. We find that the FS exhibits nesting at $\boldsymbol{q}_1 = (\pi/a, \pi/a)$ and the nesting is facilitated by heavy bands near $\bar{X}$ at $k_z = \pi/c$, originating from $c$–$f$ hybridization. The FS nesting can well explain the observed AFM excitations at $(\pi/a, \pi/a)$ from INS measurements,[12] which might be the driving force for spin-fluctuation-mediated superconductivity.[19,80] Our results further unveil the fine band splittings related to the locally noncentrosymmetric structure, a quasi-2D FS due to weak interlayer hopping and strong Kondo peaks likely caused by low-lying CEF excitations. The spectroscopic insight could be important to understand the electronic and magnetic excitations in $CeRh_2As_2$, as well as the origin of multiple superconducting phases in this enigmatic compound.

*Acknowledgements.* This work was supported by the National Key R&D Program of China (Grant Nos. 2022YFA140220 and 2023YFA1406303), the State Key Project of Zhejiang Province (Grant No. LZ22A040007), the National Natural Science Foundation of China (Grant Nos. U23A20580, 12174331, 12204159, and 12274364), the Key R&D Program of Zhejiang Province, China (Grant No. 2021C01002), and the Bridging Grant (Grant No. BG11-072020) with China, Japan, South Korea and ASEAN region funded by the Swiss State Secretariat for Education, Research and Innovation. We acknowledge MAX Ⅳ Laboratory for time on Beamline BLOCH (Proposal No. 20200306). Research conducted at MAX Ⅳ is supported by the Swedish Research Council (Contract No. 2018-07152), the Swedish Governmental Agency for Innovation Systems (Contract No. 2018-04969), and Formas (Contract No. 2019-02496). We thank Dr. Craig Polley, Ms. Dongting Zhang, Mr. Yuxin Chen and Prof. Xin Lu for experimental assistance. We are also grateful to Dr. Tong Chen, Prof. Yu Song, Prof. Michael Smidman, Prof. Philip Brydon, Dr. Seunghyun Khim and Dr. Oliver Stockert for helpful discussions.

Note: During the long review process of our paper (arXiv:2309.06732), another ARPES work on $CeRh_2As_2$, which was posted on arXiv (arXiv:2309.05895) around the same time of our paper, was recently published.[50] Another independent ARPES work, which was posted on arXiv at a later time (arXiv:2403.14057), was also published recently.[81] Our work includes a systematic comparison between ARPES spectra and DFT + DMFT calculations to illustrate the FS nesting, which was not covered by these works.

# References


[1] Khim S, Landaeta J F, Banda J, Bannor N, Brando M, Brydon P M R, Hafner D, Küchler R, Cardoso-Gil R, Stockert U, Mackenzie A P, Agterberg D F, Geibel C, and Hassinger E 2021 *Science* **373** 1012
[2] Landaeta J F, Khanenko P, Cavanagh D C, Geibel C, Khim S, Mishra S, Sheikin I, Brydon P M R, Agterberg D F, Brando M, and Hassinger E 2022 *Phys. Rev. X* **12** 031001
[3] Yoshida T, Sigrist M, and Yanase Y 2012 *Phys. Rev. B* **86** 134514
[4] Nogaki K, Daido A, Ishizuka J, and Yanase Y 2021 *Phys. Rev. Res.* **3** L032071
[5] Möckli D and Ramires A 2021 *Phys. Rev. Res.* **3** 023204
[6] Skurativska A, Sigrist M, and Fischer M H 2021 *Phys. Rev. Res.* **3** 033133
[7] Cavanagh D C, Shishidou T, Weinert M, Brydon P M R, and Agterberg D F 2022 *Phys. Rev. B* **105** L020505
[8] Schertenleib E G, Fischer M H, and Sigrist M 2021 *Phys. Rev. Res.* **3** 023179
[9] Möckli D and Ramires A 2021 *Phys. Rev. B* **104** 134517
[10] Fischer M H, Sigrist M, Agterberg D F, and Yanase Y 2022 arXiv:2204.02449 [cond-mat.supr-con]
[11] Siddiquee H, Rehfuss Z, Broyles C, and Ran S 2022 arXiv:2212.06930 [cond-mat.supr-con]
[12] Chen T, Siddiquee H, Rehfuss Z, Gao S Y, Lygouras C, Drouin J, Morano V, Avers K E, Schmitt C J, Podlesnyak A, Ran S, Song Y, and Broholm C 2024 arXiv:2406.03566 [cond-mat.str-el]
[13] Kibune M, Kitagawa S, Kinjo K, Ogata S, Manago M, Taniguchi T, Ishida K, Brando M, Hassinger E, Rosner H, Geibel C, and Khim S 2022 *Phys. Rev. Lett.* **128** 057002
[14] Khim S, Stockert O, Brando M, Geibel C, Baines C, Hicken T J, Luetkens H, Das D, Shiroka T, Guguchia Z, and Scheuermann R 2024 arXiv:2406.16575 [cond-mat.str-el]
[15] Hafner D, Khanenko P, Eljaouhari E O, Küchler R, Banda J, Bannor N, Lühmann T, Landaeta J F, Mishra S, Sheikin I, Hassinger E, Khim S, Geibel C, Zwicknagl G, and Brando M 2022 *Phys. Rev. X* **12** 011023
[16] Steglich F, Aarts J, Bredl C D, Lieke W, Meschede D, Franz W, and Schäfer H 1979 *Phys. Rev. Lett.* **43** 1892
[17] Smidman M, Stockert O, Nica E M, Liu Y, Yuan H, Si Q, and Steglich F 2023 *Rev. Mod. Phys.* **95** 031002
[18] Petrovic C, Pagliuso P G, Hundley M F, Movshovich R, Sarrao J L, Thompson J D, Fisk Z, and Monthoux P 2001 *J. Phys.: Condens. Matter* **13** L337
[19] Lee C, Agterberg D F, and Brydon P M R 2024 arXiv:2407.00536 [cond-mat.supr-con]
[20] Zwicknagl G 2016 *Rep. Prog. Phys.* **79** 124501
[21] Nogaki K and Yanase Y 2022 *Phys. Rev. B* **106** L100504
[22] Hazra T and Coleman P 2023 *Phys. Rev. Lett.* **130** 136002
[23] Machida K 2022 *Phys. Rev. B* **106** 184509
[24] Ishizuka J, Nogaki K, Sigrist M, and Yanase Y 2023 arXiv:2311.00324 [cond-mat.supr-con]
[25] Ptok A, Kapcia K J, Jochym P T, Łażewski J, Oleś A M, and Piekarz P 2021 *Phys. Rev. B* **104** L041109
[26] See the Supplementary Material, which includes Refs.[27–38] and details on crystal growth, characterizations, ARPES measurements and calculations.
[27] Ernst S, Kirchner S, Krellner C, Geibel C, Zwicknagl G, Steglich F, and Wirth S 2011 *Nature* **474** 362
[28] Wirth S and Steglich F 2016 *Nat. Rev. Mater.* **1** 16051
[29] Shen S, Qin T, Gao J, Wen C, Wang J, Wang W, Li J, Luo X, Lu W, Sun Y, and Yan S 2022 *Chin. Phys. Lett.* **39** 077401
[30] Kimura S i, Sichelschmidt J, and Khim S 2021 *Phys. Rev. B* **104** 245116
[31] Kresse G and Hafner J 1993 *Phys. Rev. B* **47** 558
[32] Kresse G and Joubert D 1999 *Phys. Rev. B* **59** 1758

[33] Perdew J P, Burke K, and Ernzerhof M 1996 *Phys. Rev. Lett.* **77** 3865
[34] Mostofi A A, Yates J R, Lee Y S, Souza I, Vanderbilt D, and Marzari N 2008 *Comput. Phys. Commun.* **178** 685
[35] Zhi G X, Xu C C, Wu S Q, Ning F L, and Cao C 2022 *Comput. Phys. Commun.* **271** 108196
[36] Haule K, Yee C H, and Kim K 2010 *Phys. Rev. B* **81** 195107
[37] Schwarz K, Blaha P, and Madsen G K H 2002 *Comput. Phys. Commun.* **147** 71
[38] Haule K 2007 *Phys. Rev. B* **75** 155113
[39] Denlinger J D, Gweon G H, Allen J W, Olson C G, Maple M B, Sarrao J L, Armstrong P E, Fisk Z, and Yamagami H 2001 *J. Electron Spectrosc. Relat. Phenom.* **117–118** 347
[40] Wu Z Z, Fang Y, Su H, Xie W, Li P, Wu Y, Huang Y B, Shen D W, Thiagarajan B, Adell J, Cao C, Yuan H Q, Steglich F, and Liu Y 2021 *Phys. Rev. Lett.* **127** 067002
[41] Sekiyama A, Iwasaki T, Matsuda K, Saitoh Y, Ônuki Y, and Suga S 2000 *Nature* **403** 396
[42] Allen J W 2005 *J. Phys. Soc. Jpn.* **74** 34
[43] Fujimori S i 2016 *J. Phys.: Condens. Matter* **28** 153002
[44] Im H J, Ito T, Kim H D, Kimura S, Lee K E, Hong J B, Kwon Y S, Yasui A, and Yamagami H 2008 *Phys. Rev. Lett.* **100** 176402
[45] Chen Q Y, Xu D F, Niu X H, Jiang J, Peng R, Xu H C, Wen C H P, Ding Z F, Huang K, Shu L, Zhang Y J, Lee H, Strocov V N, Shi M, Bisti F, Schmitt T, Huang Y B, Dudin P, Lai X C, Kirchner S, Yuan H Q, and Feng D L 2017 *Phys. Rev. B* **96** 045107
[46] Jang S, Denlinger J D, Allen J W, Zapf V S, Maple M B, Kim J N, Jang B G, and Shim J H 2020 *Proc. Natl. Acad. Sci. USA* **117** 23467
[47] Kirchner S, Paschen S, Chen Q, Wirth S, Feng D, Thompson J D, and Si Q 2020 *Rev. Mod. Phys.* **92** 011002
[48] Wu Y, Zhang Y, Du F, Shen B, Zheng H, Fang Y, Smidman M, Cao C, Steglich F, Yuan H, Denlinger J D, and Liu Y 2021 *Phys. Rev. Lett.* **126** 216406
[49] Yuan Y H, Duan Y X, Rusz J, Zhang C, Song J J, Wu Q Y, Sassa Y, Tjernberg O, Månsson M, Berntsen M H, Wu F Y, Liu S Y, Liu H, Zhu S X, Liu Z T, Zhao Y Z, Tobash P H, Bauer E D, Thompson J D, Oppeneer P M, Durakiewicz T, and Meng J Q 2021 *Phys. Rev. B* **103** 125122
[50] Chen X Z, Wang L, Ishizuka J, Zhang R J, Nogaki K, Cheng Y W, Yang F Z, Chen Z H, Zhu F Y, Liu Z T, Mei J W, Yanase Y, Lv B Q, and Huang Y B 2024 *Phys. Rev. X* **14** 021048
[51] Cameron A S, Friemel G, and Inosov D S 2016 *Rep. Prog. Phys.* **79** 066502
[52] Koitzsch A, Heming N, Knupfer M, Büchner B, Portnichenko P Y, Dukhnenko A V, Shitsevalova N Y, Filipov V B, Lev L L, Strocov V N, Ollivier J, and Inosov D S 2016 *Nat. Commun.* **7** 10876
[53] Jang D, Portnichenko P Y, Cameron A S, Friemel G, Dukhnenko A V, Shitsevalova N Y, Filipov V B, Schneidewind A, Ivanov A, Inosov D S, and Brando M 2017 *npj Quantum Mater.* **2** 62
[54] Chen Q Y, Wen C H P, Yao Q, Huang K, Ding Z F, Shu L, Niu X H, Zhang Y, Lai X C, Huang Y B, Zhang G B, Kirchner S, and Feng D L 2018 *Phys. Rev. B* **97** 075149
[55] Ehm D, Hüfner S, Reinert F, Kroha J, Wölfle P, Stockert O, Geibel C, and Löhneysen H V 2007 *Phys. Rev. B* **76** 045117
[56] Patil S, Generalov A, Güttler M, Kushwaha P, Chikina A, Kummer K, Rödel T C, Santander-Syro A F, Caroca-Canales N, Geibel C, Danzenbächer S, Kucherenko Y, Laubschat C, Allen J W, and Vyalikh D V 2016 *Nat. Commun.* **7** 11029
[57] Christovam D S, Ferreira-Carvalho M, Marino A, Sundermann M, Takegami D, Melendez-Sans A, Tsuei K D, Hu Z W, Rößler S, Valvidares M, Haverkort M W, Liu Y, Bauer E D, Tjeng L H, Zwicknagl G, and Severing A 2024 *Phys. Rev. Lett.* **132** 046401
[58] Liu Y 2021 *Sci. China Phys. Mech. Astron.* **64** 127431
[59] McElroy K, Gweon G H, Zhou S Y, Graf J, Uchida S, Eisaki H, Takagi H, Sasagawa T, Lee D H, and Lanzara A 2006 *Phys. Rev. Lett.* **96** 067005
[60] Chatterjee U, Shi M, Kaminski A, Kanigel A, Fretwell H M, Terashima K, Takahashi T, Rosenkranz S, Li Z Z, Raffy H, Santander-Syro A, Kadowaki K, Norman M R, Randeria M, and Campuzano J C 2006 *Phys. Rev. Lett.* **96** 107006
[61] Shen D W, Xie B P, Zhao J F, Yang L X, Fang L, Shi J, He R H, Lu D H, Wen H H, and Feng D L 2007 *Phys. Rev. Lett.* **99** 216404
[62] Eremin I, Zwicknagl G, Thalmeier P, and Fulde P 2008 *Phys. Rev. Lett.* **101** 187001
[63] Stockert O, Arndt J, Faulhaber E, Geibel C, Jeevan H S, Kirchner S, Loewenhaupt M, Schmalzl K, Schmidt W, Si Q, and Steglich F 2011 *Nat. Phys.* **7** 119
[64] Sato N K, Aso N, Miyake K, Shiina R, Thalmeier P, Varelogiannis G, Geibel C, Steglich F, Fulde P, and Komatsubara T 2001 *Nature* **410** 340
[65] Stockert O and Steglich F 2023 *Physica C* **615** 1354375
[66] Mydosh J A and Oppeneer P M 2011 *Rev. Mod. Phys.* **83** 1301
[67] Ikeda H, Suzuki M T, Arita R, Takimoto T, Shibauchi T, and Matsuda Y 2012 *Nat. Phys.* **8** 528
[68] Wang X, Gong D, Liu B, Ma X, Zhao J, Wang P, Sheng Y, Guo J, Sun L, Zhang W, Lai X, Tan S, Yang Y F, and Li S 2022 *Chin. Phys. Lett.* **39** 107101
[69] Broholm C, Kjems J K, Buyers W J L, Matthews P, Palstra T T M, Menovsky A A, and Mydosh J A 1987 *Phys. Rev. Lett.* **58** 1467
[70] Broholm C, Lin H, Matthews P T, Mason T E, Buyers W J L, Collins M F, Menovsky A A, Mydosh J A, and Kjems J K 1991 *Phys. Rev. B* **43** 12809
[71] Wiebe C R, Janik J A, MacDougall G J, Luke G M, Garrett J D, Zhou H D, Jo Y J, Balicas L, Qiu Y, Copley J R D, Yamani Z, and Buyers W J L 2007 *Nat. Phys.* **3** 96
[72] Santander-Syro A F, Klein M, Boariu F L, Nuber A, Lejay P, and Reinert F 2009 *Nat. Phys.* **5** 637
[73] Boariu F L, Bareille C, Schwab H, Nuber A, Lejay P, Durakiewicz T, Reinert F, and Santander-Syro A F 2013 *Phys. Rev. Lett.* **110** 156404
[74] Chatterjee S, Trinckauf J, Hänke T, Shai D E, Harter J W, Williams T J, Luke G M, Shen K M, and Geck J 2013 *Phys. Rev. Lett.* **110** 186401
[75] Meng J Q, Oppeneer P M, Mydosh J A, Riseborough P S, Gofryk K, Joyce J J, Bauer E D, Li Y, and Durakiewicz T 2013 *Phys. Rev. Lett.* **111** 127002
[76] Yoshida R, Nakamura Y, Fukui M, Haga Y, Yamamoto E, Ōnuki Y, Okawa M, Shin S, Hirai M, Muraoka Y, and Yokoya T 2010 *Phys. Rev. B* **82** 205108
[77] Zhang W, Lu H Y, Xie D H, Feng W, Tan S Y, Liu Y, Zhu X G, Zhang Y, Hao Q Q, Huang Y B, Lai X C, and Chen Q Y 2018 *Phys. Rev. B* **98** 115121
[78] Denlinger J D, Kang J S, Dudy L, Allen J W, Kim K, Shim J H, Haule K, Sarrao J L, Butch N P, and Maple M B 2022 *Electron. Struct.* **4** 013001
[79] Mishra S, Liu Y, Bauer E D, Ronning F, and Thomas S M 2022 *Phys. Rev. B* **106** L140502
[80] Scalapino D J 2012 *Rev. Mod. Phys.* **84** 1383
[81] Chen B, Liu H, Wu Q Y, Zhang C, Ye X Q, Zhao Y Z, Song J J, Tian X Y, Tan B L, Liu Z T, Ye M, Chen Z H, Huang Y B, Shen D W, Yuan Y H, He J, Duan Y X, and Meng J Q 2024 *Phys. Rev. B* **110** L041120